Pharmacological Research 185 (2022) 106516

Contents lists available at ScienceDirect

Pharmacological Research

journal homepage: www.elsevier.com/locate/yphrs

Morpho-functional analysis of the early changes induced in retinal ganglion cells by the onset of diabetic retinopathy: The effects of a neuroprotective strategy

Rosario Amato [a,1], Elisabetta Catalani [b,1], Massimo Dal Monte [a,c], Maurizio Cammalleri [a,c], Davide Cervia [b,*], Giovanni Casini [a,c,**]

[a] Department of Biology, University of Pisa, Pisa, Italy
[b] Department for Innovation in Biological, Agro-Food and Forest Systems (DIBAF), University of Tuscia, Viterbo, Italy
[c] Interdepartmental Research Center Nutrafood "Nutraceuticals and Food for Health", University of Pisa, Pisa, Italy

ARTICLE INFO

Keywords:
Hyperglycemia
Octreotide
Somatostatin
Dendritic tree
Electroretinography
Morphometric analysis

ABSTRACT

Purpose: Retinal ganglion cells (RGCs) are highly susceptible to diabetes-induced metabolic stress. This study describes the early responses of RGCs to hyperglycemia and examines the effects of the neuroprotective somatostatin analog octreotide (OCT).
Methods: Thy1-green fluorescent protein (GFP)-M transgenic mice were used, which express GFP in a number of RGCs. OCT was intravitreally injected in mice with streptozotocin (STZ)-induced diabetes. A longitudinal electroretinography (ERG) analysis was performed up to 2 weeks from STZ treatment. RGC density was measured and extensive morphometric analyses were performed on identified RGC subtypes.
Results: STZ treatment caused a decline of RGC function, which was counteracted by OCT. No differences in RGC density were recorded, indicating that impaired activity was unlikely to be related to RGC death. Different GFP-labeled RGC subtypes were identified and analyzed. Overall, large RGCs were mostly affected by diabetes and responded to OCT treatment, while those with smaller dendritic arborizations were less involved. Interestingly, depending on the complexity of the dendritic tree, OCT could completely rescue RGC morphometric parameters or increase the effects of hyperglycemia.
Conclusions: There is an early response of RGCs to diabetes, which involves specific morpho-functional deficits but not overt cell death. OCT induces adaptive changes that, although different among RGC subtypes, contribute to RGC functionality in the presence of metabolic stress. These results highlight the importance of neuronal protection in the early phases of diabetic retinopathy, when cell loss has not yet started and RGC morphology can be preserved or adjusted to maintain RGC physiology.

1. Introduction

Retinal ganglion cells (RGCs) cover a crucial role in addressing the retinal signaling towards the central visual pathways, and alterations in their functional or structural properties often imply severe consequences for vision [1]. Indeed, primary damage to RGCs has been recognized as the main pathological feature of a number of sight-threatening diseases such as glaucoma, age-related macular degeneration, and optic neuropathies [2–4]. RGC damage is likely to occur because these cells stand on a metabolic edge that renders them prominently vulnerable to local and/or systemic metabolic stressors [5]. This is particularly evident in diabetic conditions, in which hyperglycemia-driven biochemical

Abbreviations: DR, diabetic retinopathy; ERG, electroretinogram; GFP, green fluorescent protein; IPL, inner plexiform layer; OCT, octreotide; OPs, oscillatory potentials; PB, phosphate buffer; PERG, pattern ERG; phERG, photopic ERG; phNR, photopic negative response; RGC, retinal ganglion cell; scERG, scotopic ERG; STZ, streptozotocin.

* Correspondence to: Department for Innovation in Biological, Agro-Food and Forest Systems (DIBAF), University of Tuscia, largo dell'Università snc, 01100 Viterbo, Italy.
** Correspondence to: Department of Biology, University of Pisa, via San Zeno 31, 56127 Pisa, Italy.
E-mail addresses: d.cervia@unitus.it (D. Cervia), giovanni.casini@unipi.it (G. Casini).
[1] Rosario Amato and Elisabetta Catalani have equal contribution to this study.

https://doi.org/10.1016/j.phrs.2022.106516
Received 1 September 2022; Received in revised form 5 October 2022; Accepted 14 October 2022
Available online 19 October 2022

alterations, together with excitotoxicity and neurotrophin depletion, promote neurodegenerative phenomena characterizing the early stages of diabetic retinopathy (DR) and likely preceding vascular abnormalities [6,7].

Evidence of RGC damage in DR, characterized by RGC depletion and decreased thickness of the nerve fiber layer, has been reported both in patients and in animal models [8,9]. Interestingly, RGC damage may also affect the inner plexiform layer (IPL), which appears to be reduced due to alterations and/or loss of dendrites and synapses of different RGC subtypes [10]. Indeed, morphological alterations of RGC dendritic arbors may reflect RGC suffering and functional damage. RGC dendrites may be "monostratified", confined to one layer (sublamina) of the IPL, or "bistratified", distributed into two layers. OFF-type, monostratified RGCs have their dendrites predominantly in the outer IPL sublamina, while ON-type RGCs arborize in the inner IPL sublamina. Bistratified RGCs belong to the ON/OFF-type and have arborizations in both IPL sublaminae [1]. Changes in RGC arborizations have been observed in chronic conditions, such as in diabetic human retinas and in retinas of diabetic rodents [11–13]. In particular, the dendrites of ON-type RGCs have been reported to be mostly affected in mice at 3 months after streptozotocin (STZ)-induced diabetes, and these changes corresponded to significant alterations in functional RGC activity [14]. Interestingly, electroretinographic features that are likely to be linked to RGC activity seem to be also affected very early in DR. For instance, oscillatory potentials (OPs), which are related to the activity of third order neurons (including amacrine cells and RGCs), were the components of the electroretinogram (ERG) showing the most precocious alterations in the progression of DR in STZ-treated mice [15].

Considering the high vulnerability of RGCs to metabolic insults, it is reasonable to hypothesize that these cells are primarily affected in their morpho-functional features during the very early stages of DR, before cellular death becomes manifest. Since a crucial point for therapies preventing DR is to avoid or mitigate retinal neurodegeneration, it is important that neuroprotective treatments are aimed not only at protecting from neuronal death but also at preserving dendritic arborizations and functional activity of RGCs. Additionally, the early detection of diabetes-driven neuronal suffering acquires a key importance since a timely intervention could be effective in preventing the disequilibrium in neurovascular communication factors that are likely to promote vasculopathy, according to a hypothesis that we have investigated and discussed previously [16–18]. In this context, we found that octreotide (OCT), an octapeptide somatostatin analog with strong neuroprotective properties, is highly effective in protecting retinal cells from a variety of insults [19–23]. OCT has been the first marketed somatostatin receptor ligand and is commonly prescribed off-label in DR and diabetic macular edema [24].

In the present study, we asked whether physiological deficits concomitant with morphological alterations of specific RGC subtypes could be detected in the very early phases of DR, before the occurrence of significant cell death, and to what extent a very precocious, neuroprotective treatment with OCT could slow down or inhibit the morpho-functional decline of RGCs. To this aim, diabetes was induced with a STZ injection in Thy1-green fluorescent protein (GFP)-M transgenic mice [25], which express GFP in a number of heterogeneous RGC subtypes. The functional activity of RGCs was longitudinally monitored up to two weeks after STZ administration (endpoint) using scotopic ERG (scERG), photopic ERG (phERG) and pattern ERG (PERG) recordings. In addition, an extensive morphometric assessment of RGCs was performed at endpoint using confocal microscopy to reconstruct and analyze RGC morphologies.

2. Materials and methods

2.1. Animals and treatments

The Thy1-GFP-M mice were a kind gift from E. Strettoi (Institute of Neuroscience, National Council of Research, Pisa, Italy) [26]. They are homozygous for the Thy1-GFP allele and were derived by breeding from the B6.Cg-Tg(thy1-GFP)/J strain originally devised by J.R. Sanes [25]. The mice were five-week-old and they were kept in a regulated environment (23 ± 1 °C, 50 ± 5% humidity) with a 12 h light/dark cycle (lights on at 8:00 a.m.). All the procedures were performed in compliance with the ARVO Statement for the Use of Animals in Ophthalmic and Vision Research, the EU Directive (2010/63/EU), and the Italian guidelines for animal care (DL 26/14; Permission number: 132/2019-PR).

A total of 36 mice were used in these studies, distributed according to the following experimental protocol: at baseline, 18 mice received a single intraperitoneal injection of 150 mg/kg STZ (Sigma-Aldrich) dissolved in citrate buffer, pH 4.5. Control mice received an equivalent volume of the citrate buffer solution. Three days after STZ injection, 9 mice from the STZ-treated group were randomly assigned to the OCT treatment group and intravitreally injected with 1 μl of an OCT (Sigma-Aldrich) solution containing an amount of OCT to reach a final intravitreal OCT concentration of about 1 mM (considering a vitreous volume of 5 μl). According to previous studies, 1 mM OCT is a concentration giving maximal receptor occupancy in different systems [27–30], including the mouse retina [20,31,32]. Nine mice from the control group were also intravitreally injected with OCT. Control animals that did not receive the OCT treatment were intravitreally injected with 1 μl saline. The intravitreal injections were performed in mice anesthetized with an intraperitoneal injection of Avertin (1.25% avertin/g body weight) using a microsyringe (NanoFil syringe; World Precision Instruments, Sarasota, FL, USA) equipped with a 36-gauge needle. For a summary of the experimental groups, see Supplementary Table 1. No differences were recorded in any of the parameters analyzed in these studies between saline-injected and OCT-injected control mice. Therefore, for the sake of simplicity, the data reported hereafter will be referred only to control mice, mice treated with STZ (STZ mice) and mice treated with both STZ and OCT (STZ+OCT mice).

Non-fasting glycemia, measured by tail sampling using a OneTouch Ultra glucometer (LifeScan Inc., Milpitas, CA, USA), and body weight were monitored at baseline, at three days and one week after STZ injection, and at endpoint, when the mice were sacrificed by cervical dislocation and their retinas used for quantification of RGC numbers or for the analysis of RGC morphologies. The treatment / testing paradigm is summarized in Fig. 1A.

2.2. Longitudinal electrophysiological assessment of retinal activity

ERG recordings were performed at baseline, at 3 (before OCT injection) and 7 days from baseline, and at endpoint. At each time-point, the mice were subjected to a recording routine that included an analysis of the rod pathway with scERG, an analysis of the cone pathway with phERG, and an analysis of RGC activity with PERG. After overnight dark-adaption, the mice were anesthetized with an intraperitoneal injection of Avertin (1.25% avertin/g body weight) and gently restrained in a custom-made stereotaxic apparatus allowing an unobstructed visual field. Body temperature was maintained at 37 °C by mean of a feedback-controlled heating pad and corneal moisture was ensured by adding balanced saline solution before and during the recording session. The recording electrodes, consisting of 0.2 mm loop-shaped silver wires, were carefully laid on the corneal surface of each eye using micro manipulators. Stainless steel needles were used as reference electrodes, one for each eye, and ground electrode, and inserted subcutaneously on the mouse scalp and at the tail root, respectively. In each recording session, scERG was performed first using a commercially available ERG setup (Retimax Advanced, CSO, Firenze, Italy) and a 10 cd·s/m^2 flash stimulus delivered with a Ganzfeld bowl. Five consecutive signals recorded simultaneously from each eye were averaged to reduce noise after amplification (5000-fold) and band-pass filtered (1–100 Hz). In the deriving waveform, the amplitude of the a-wave (baseline to trough)

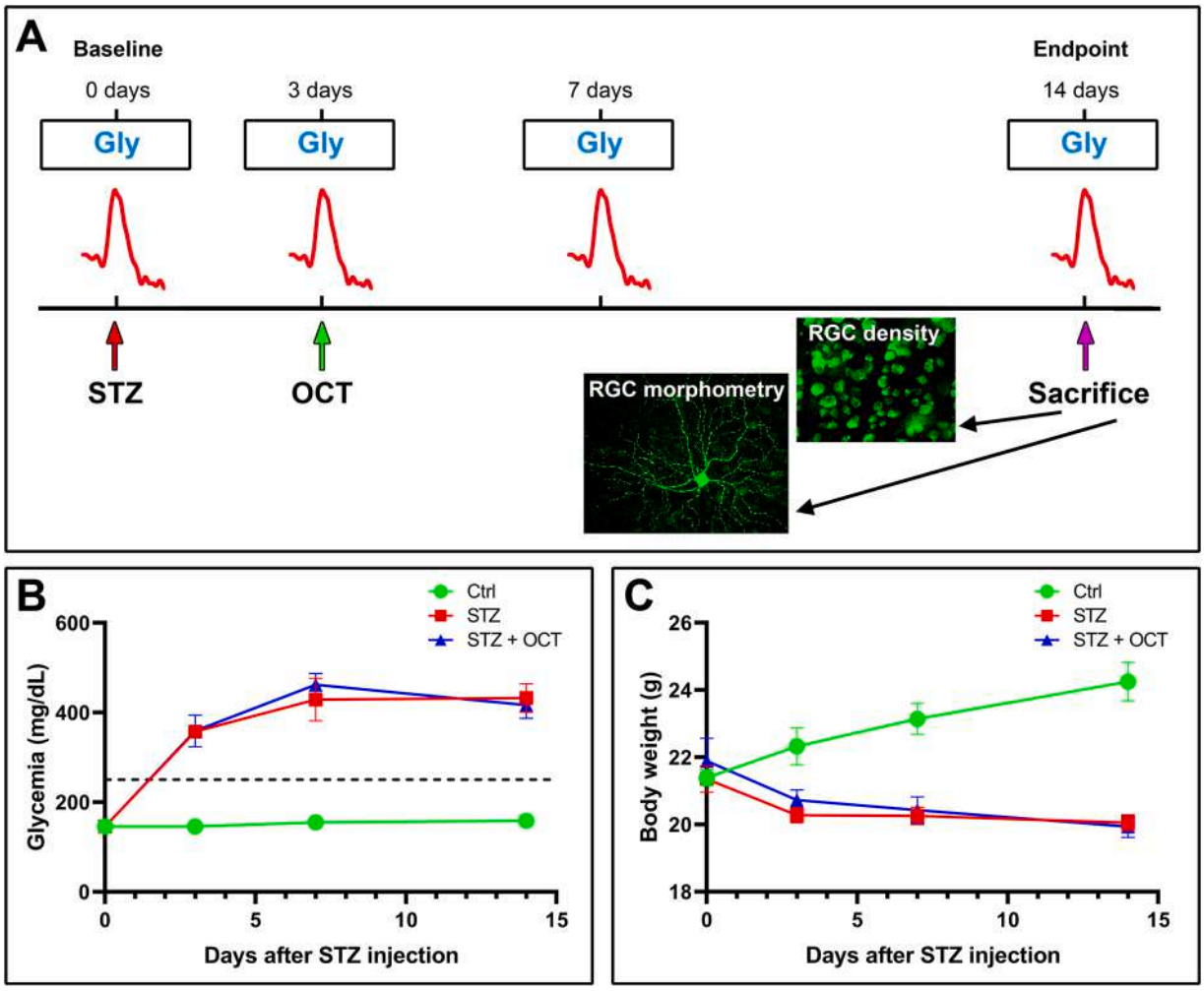

Fig. 1. (A) Treatment / testing paradigm of the study. At baseline, the mice were injected with STZ, while after 3 days they were intravitreally injected with OCT. Measurements of glycemia (Gly) and ERG recordings (indicated by the red waveform) were performed at baseline, at 3, 7, and 14 days (endpoint) after STZ injection. At endpoint, the mice were sacrificed and used to determine RGC density or to perform RGC morphometric analyses. The glycemia and the body weight of the mice during the experimental period are shown in (B) and in (C), respectively. The dashed line in (B) indicates glycemia = 250 mg/dL. Mean ± SEM, N = 6.

and that of the b-wave (trough to peak) were measured. OPs were isolated from each endpoint scERG recording by band-pass filtering of 65–300 Hz to exclude interference from the a- and b-wave. The amplitudes of the main OPs (OP1, OP2 and OP3) were measured from the corresponding peaks to the preceding troughs, according to the ISCEV guidelines [33].

Immediately after the scERG session, the mice were light-adapted by exposing them to 40.0 cd·s/m^2, rod-saturating, green background light, delivered with a Ganzfeld bowl, for one minute. Thereafter, cone pathway stimulation was obtained by delivering 5 cd·s/m^2 flashlight stimuli on the same adaptation background. The phERG responses simultaneously recorded from both eyes were amplified (5000-fold) and band-pass filtered (1–100 Hz). The waveform deriving from the average of 50 consecutive responses was analyzed for the b-wave (baseline to peak) and the photopic negative response (baseline to trough).

The phERG session was followed by PERG recordings. Using the same electrode setup, a visual stimulus consisting of black and white (98% contrast) bars contrast-reversing at 1 Hz temporal frequency and 0.05 cyc/deg spatial frequency was administered with a 19'' light emitting diode display (area: 74°x 62°) aligned to the mouse cornea and spaced 25 cm from the mouse eye. Each pattern reversal-deriving signal was amplified (10,000-fold) and band-pass filtered (1–30 Hz). Overall, the responses deriving from 900 consecutive pattern reversals were averaged to reduce noise contamination by a factor of $\sqrt{900} = 30$. PERG responses were analyzed by detecting the early positive inflection point (N35), the positive peak (P50), and the belated negative trough (N95) in each PERG waveform. Given the proportional variation of the positive (N35-P50) and the negative (P50-N95) components of the PERG response (Supplementary Fig. 1), the P50-N95 amplitude (hereinafter referred as PERG amplitude) was chosen as the main analytical parameter for the longitudinal PERG analysis, in order to optimize both the dynamic range of measures and the signal-to-noise ratio. Implicit time of the PERG response was also longitudinally analyzed as time-to-P50 (hereinafter referred as PERG latency).

2.3. Immunofluorescence

The mice were sacrificed by cervical dislocation. Their eyes were dissected and immersion fixed in cold 4% paraformaldehyde in 0.1 M phosphate buffer (PB) for 1 h at room temperature and then stored in 25% sucrose in PB at 4 °C for at least 24 h. The retinas were then dissected, freeze thawed, washed in PB, and pre-treated with 5% BSA in PB containing 0.5% Triton X-100 for 6 h at 4 °C. The retinas used for quantification of RGC density were incubated with a guinea pig polyclonal antibody directed to RNA-binding protein with multiple splicing (RBPMS, ABN1376, Merck, Darmstadt, Germany; dilution 1:100), a RGC marker [34], for three days at 4 °C. Subsequently, they were incubated in appropriate Alexa Fluor secondary antibodies diluted in PB

containing 1% BSA and 0.1% Triton X-100 for two days at 4 °C. The retinas used for morphometric analyses were incubated with a GFP Polyclonal Antibody-Alexa Fluor 488 conjugated (# A-21311; Invitrogen - Thermo Fisher Scientific, Waltham, MA USA), diluted 1:500 in PB containing 1% BSA and 0.1% Triton X-100 for four days at 4 °C, to enhance the signal of fluorescent RGCs. All retinas were then flat mounted on polarized glass slides with the RGC layer facing up and coverslipped.

2.4. RGC counting

Images of RBPMS immunolabeled RGCs were acquired with a Zeiss Axioskop 2 plus microscope equipped with an Axiocam 503 color photocamera and the Axiovision software (Carl Zeiss, Oberkochen, Germany). Image sampling was performed in order to obtain 4 radial tiles (440 ×330 μm) in central and peripheral retina (center: 500 μm from the optic nerve head; periphery: 500 μm from the peripheral edge). RGC density was measured as the average of the number of RBPMS immunopositive somata per mm^2. Three retinas from three different mice in each experimental group were used for this analysis.

2.5. RGC morphometry

Images of GFP-labeled RGCs were acquired from flat mounts of Thy1-GFP-M mice using a Zeiss LSM 710 confocal microscope and an EC Plan-Neofluar 40x/1.30 Oil DIC M27 at a resolution of 1024 × 1024 pixels. The distance between adjacent focal planes was set at 1 μm. Acquired Z-stacks included the whole ganglion cell layer and the IPL. A total of 4 out of 6 retinas in each experimental group (each retina belonged to a different animal) were examined to assess the morphometric features of the RGCs. Images of all labeled RGCs in the retinas chosen for analysis were saved and analyzed off-line. A quantitative morphometric analysis was performed on those RGC subtypes in which at least 4 RGCs in each experimental group could be unequivocally identified as members of that subtype. Three-dimensional reconstructions of RGCs, skeletonization and morphometric measures were performed using the ImageJ software (U. S. National Institutes of Health, Bethesda, Maryland, USA). The images were adjusted for brightness and contrast using ImageJ and the figures were prepared using Adobe Photoshop (Adobe Photoshop CS3; Adobe Systems, Mountain View, CA, USA). The following morphometric characteristics were quantified for each RGC (Supplementary Fig. 2 shows some examples of image manipulation to obtain morphometric data; for details about skeleton analysis and shape descriptors used in ImageJ, see the web pages https://imagej.net/plugins/analyze-skeleton/ and https://imagej.nih.gov/ij/plugins/descriptors.html): 1) soma area; 2) soma circularity; 3) dendrite area as the area of a polygon drawn around a 2D projection of the whole dendritic arbor as shown in Supplementary Fig. 2B; 4) dendrite area as the area of the convex hull around the dendritic arbor; 5) circularity of the polygon drawn around a 2D projection of the whole dendritic arbor (see point 3); 6) circularity of the convex hull around the dendritic arbor (see point 4); 7) number of dendritic branches; 8) maximum branch length; 9) average branch length; 10) number of junctions; 11) number of junction voxels; 12) number of end-point voxels; 13) number of slab voxels; 14) number of triple points; 15) number of quadruple points.

2.6. Statistical analysis

Data displaying the effect of one categorical variable (treatment) were analyzed using either Student's *t*-test, for single comparisons, or one-way analysis of variance (ANOVA) followed by Tukey's post-hoc test, for multiple comparisons. Data describing the effect of two combined categorical variables (treatment and time) were analyzed using two-way ANOVA with Bonferroni post-hoc test. The subtype specific RGC morphometry was assessed by preliminarily sorting each RGC subtype by sample size. Hence, RGC subtypes displaying a sample size $N < 5$ in each experimental group were systematically excluded from the morphometric analyses in order to select statistically significant observations for a minimal effect size ($f = 0.7$) with α error $= 0.05$ and 1-β power $= 0.08$. The results were graphed using Prism 5.03 (GraphPad software, San Diego, CA, USA).

3. Results

3.1. Glycemia and body weight

Normal blood glucose levels ranged between 132 and 167 mg/dL from baseline to endpoint, and they were significantly higher in STZ and in STZ+OCT mice starting at three days after STZ treatment (Fig. 1B). The body weight of control mice ranged between 20.2 g and 26.0 g and it was consistently lower in STZ and in STZ+OCT mice starting at three days after STZ treatment (Fig. 1 C). These results indicate the appearance of early diabetogenic effect of STZ, as for instance weight loss and prolonged hyperglycemia (blood glucose levels > 250 mg/dL), and the absence of major metabolic effects induced by intravitreally injected OCT within the experimental framework.

3.2. RGC function was impaired by hyperglycemia and recovered by OCT

The electroretinographic routine displayed in Fig. 2 was designed to obtain a comprehensive evaluation of the retinal function over time including dark- and light-adapted activity of photoreceptoral, post-receptoral and RGC activity. The ERG analysis was not significantly influenced by the procedure used for intravitreal injections, since pre- and post-injection ERG recordings, obtained following the longitudinal protocol, resulted statistically comparable, both in saline- and in OCT-injected mice. As shown in Fig. 2 A, the analysis of scERG responses among the experimental groups did not reveal any significant alteration over-time in the amplitudes of either the a-wave (Fig. 2B), referring to the overall photoreceptoral activity, or the b-wave (Fig. 2 C), reflecting the overall post-receptoral response including bipolar cell and Müller cell activity. In contrast, OP retrieval from the scERG responses at endpoint (Fig. 2D) revealed a constitutive decrement in the amplitudes of OP1, OP2 and OP3 in the STZ group (Fig. 2E), while no significant changes in their implicit time was evident (Fig. 2 F). The treatment with OCT partially prevented the STZ-induced alterations in OP1 and OP3, while it induced full recovery to control levels in OP2. Similarly, the evaluation of the phERG b-wave (Fig. 2 G) did not show any time-dependent variation following STZ injection, either with or without OCT administration, as compared to the control group (Fig. 2H). The photopic negative response (PhNR) amplitude, generally related to RGC activity, resulted slightly altered in the STZ group with an evident, although not statistically significant, tendency to decrease from the 7th day after STZ injection to endpoint, while it was unaltered in the control as well as in the STZ+OCT groups in the same time window (Fig. 2I). The analysis of the PERG response (Fig. 2 J), considered as a sensitive measure of RGC activity, demonstrated a time-dependent alteration of the peak -to-trough amplitude in STZ mice, resulting in a 46% loss at the endpoint as compared to control group (Fig. 2 K). Instead, in the STZ mice treated with OCT, the PERG amplitude was maintained over time and was significantly higher than that in STZ mice and comparable to control levels. The differences in PERG amplitude among groups did not correlate with a significant variation in PERG latency, which was consistently maintained over time in control, STZ, and STZ+OCT groups (Fig. 2 L).

3.3. RGC density at endpoint was similar in the three experimental groups

As shown in Fig. 3A-D, RGC density in central and in peripheral retinal regions did not differ significantly between control, STZ, and STZ+OCT mice. In all experimental groups, RGC densities in central retina were around 4400 RCGs/mm^2, while in retinal periphery they

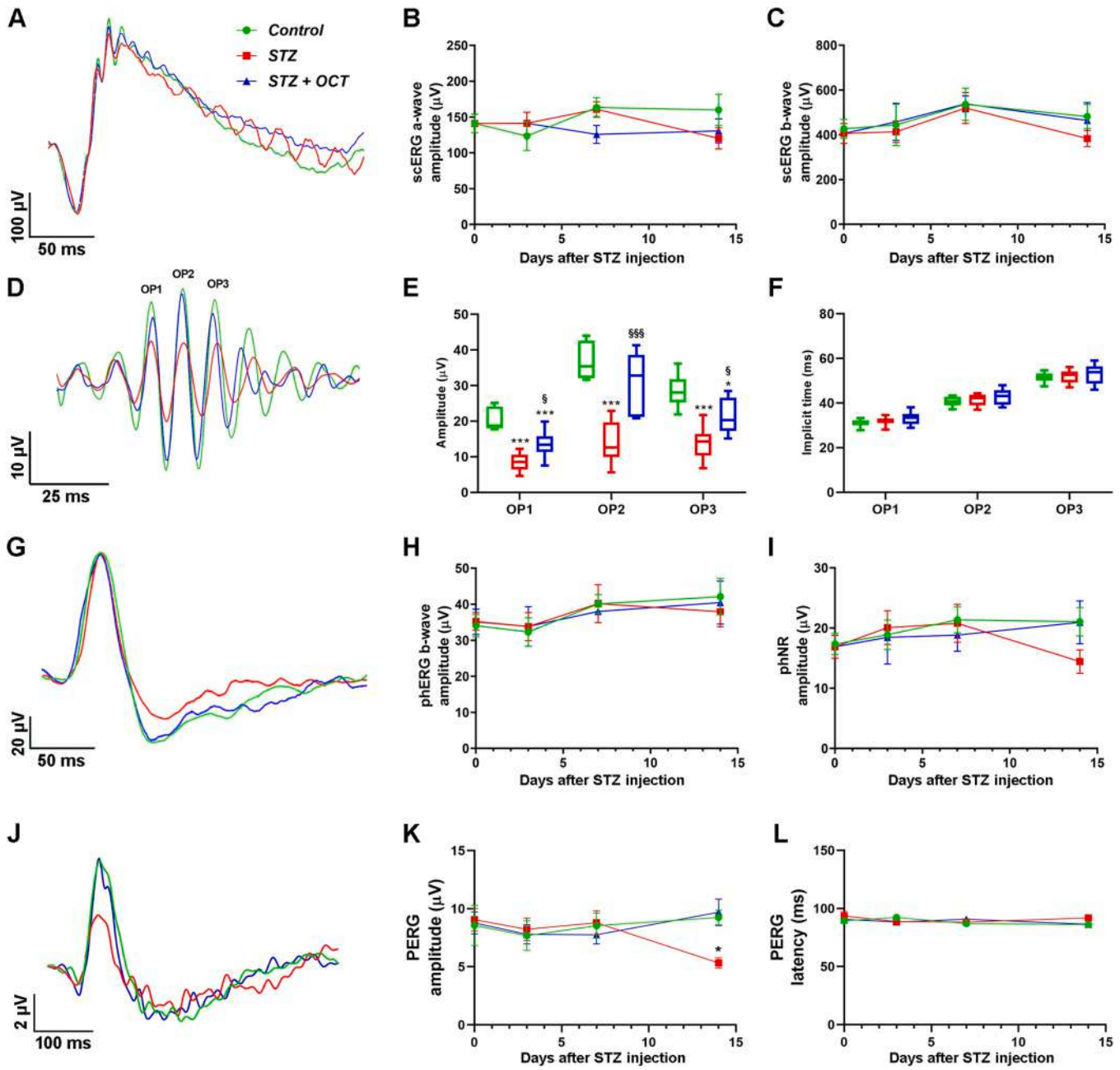

Fig. 2. Longitudinal analysis of time-dependent variations in retinal activity. (A) Representative recordings of scERG responses at endpoint in control, STZ, and STZ+OCT mice. No statistically significant alterations over time were observed in the three groups relative to the amplitudes of either the a-wave (B) or the b-wave (C). (D) Representative waveforms of the OPs retrieved from the scERG responses at endpoint. STZ mice displayed a consistent decrease in OP1, OP2 and OP3 amplitudes (E) as compared to controls, while the treatment with OCT prevented, totally or in part, this effect. No significant alterations were observed among groups relative to OP implicit time (F). (G) Representative recordings of phERG responses in control, STZ, and STZ+OCT mice at endpoint. No statistically significant alterations over time were observed in the three groups relative to the b-wave amplitude (H) or to the PhNR amplitude (I). (J) Representative recordings of PERG responses in control, STZ, and STZ+OCT mice at endpoint. STZ mice showed a time-dependent reduction of the peak-to-trough amplitude (K) with respect to the control group. STZ+OCT mice displayed a PERG amplitude that was significantly higher than that of STZ mice and statistically comparable to that of controls. No statistically significant alterations over time were observed in the three groups relative to PERG latency (L). For the longitudinal analysis of scERG, phERG and PERG responses, the statistical significance was assessed by two-way ANOVA followed by Bonferroni multiple comparison post-hoc test (mean ± SEM, N = 5). The endpoint differences in OP amplitudes and latencies were assessed by one-way ANOVA followed by Tukey's multiple comparison post-hoc test (box plots, N = 5). *$p < 0.05$, * **$p < 0.001$ vs control; $^{§}p < 0.05$, $^{§§§}p < 0.001$ vs STZ.

were around 3700 RCGs/mm^2, demonstrating the absence of significant RGC loss in the retinas of STZ or STZ+OCT mice.

3.4. OCT significantly reduced RGC damage induced by STZ treatment

In Thy1-GFP-M mice, a highly variable, small number of RGCs expressed GFP. The visibility of these cells in flat mounted retinas was increased using a fluorescent antibody directed to GFP (Supplementary Fig. 3), allowing a reliable morphometric RGC evaluation, as detailed in the methods, using a systematic confocal laser scanning microscopy analysis. More labeled RGCs were detected in control retinas than in the retinas of the STZ or the STZ+OCT group, but the differences were not

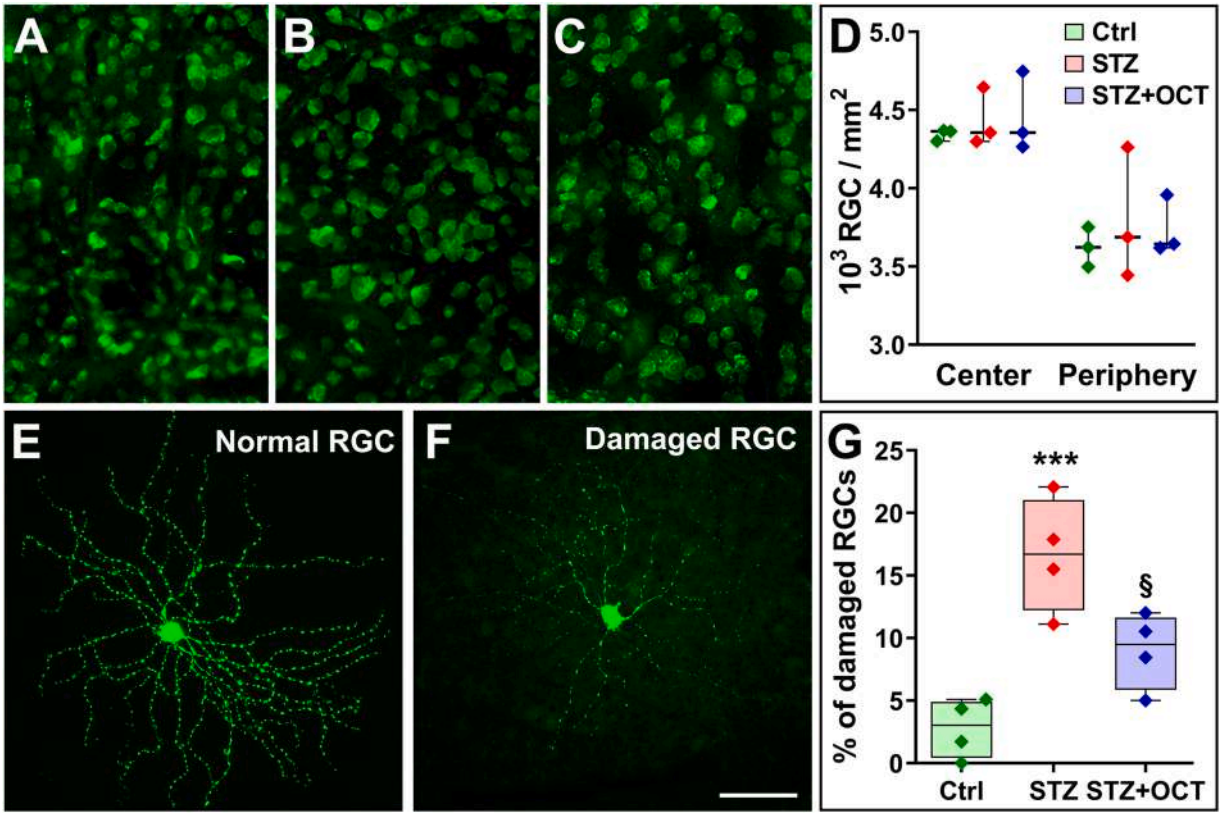

Fig. 3. RBPMS immunolabeled RGCs in central retinal regions of control (A), STZ (B) and STZ+OCT (C) mouse retinas. (D) Box and violin graph showing the RGC densities recorded in central and in peripheral retina of control, STZ, and STZ+OCT mice. (E) Representative GFP-immunopositive RGC in the retina of a control mouse in comparison to a damaged RGC in the retina of a STZ mouse (F). Scale bar, 50 μm. (G) Box and violin graph showing the percentages of damaged RGCs in the retinas used for morphometric analyses of control, STZ, and STZ+OCT mice. Statistical significance was assessed by one-way ANOVA followed by Tukey's multiple comparison post-hoc test. N = 3. * **$p < 0.001$ vs control; §$p < 0.05$ vs STZ.

statistically significant (Supplementary Fig. 4A).

As a first step, we tried to get a general idea of the effect of diabetes induction and of the treatment with OCT by determining the amount of "damaged" RGCs in the four retinas per experimental group chosen for analysis. Damaged RGCs were identified as cells with clearly reduced dendrite ramifications, less sharply defined varicosities, and faint immunofluorescence (Fig. 3E-F). For this analysis, we did not use automated computer-assisted quantifications, but the blind examination of the retinas by at least three independent observers, who took note of every "damaged" RGC they could find in each retina. The results indicated that the STZ treatment induced an about four-fold increase of damaged RGCs, while the treatment with OCT significantly reduced this harmful effect (Fig. 3 G).

3.5. *The effects of STZ and of the treatment with OCT were RGC subtype-specific*

Assignment of each RGC to a specific subtype was evaluated based on morphometric parameters, including soma shape and size, dendritic field area, number of main dendrites, dendritic arbor morphology, and stratification of dendrites in the IPL, as reported in previous papers [35–39]. The nomenclature proposed by Völgyi et al. [39] was adopted. Among the RGCs detected in control retinas, seventeen different subtypes could be identified and, with the exception of the G8 subtype (of which only two cells were detected), they are represented in Fig. 4.

Damaging effects of the STZ treatment could be easily appreciated in most of the RGC subtypes (Supplementary Fig. 5). The number of RGCs in the different subtypes and of those whose subtype could not be determined, as well as the number of analyzed RGCs in the retinas considered for analysis, are reported in Supplementary Tables 2 and 3.

The G5, G8, and G11 subtypes were excluded from the morphometric analyses since less than 4 RGCs in each experimental group could be unequivocally identified as members of those subtypes. In addition, in the cases in which two RGC subtypes shared similar characteristics, it was difficult, especially in STZ and in STZ+OCT retinas, to assign a RGC to a subtype or to the other. Therefore, in the morphometric analyses both subtypes were grouped together. This was the case of G2 and G10, of G3 and G7, of G13 and G14, and of G16 and G17 RGCs. In most cases, the number of RGCs considered for morphometric analysis in a given subtype was lower than the number of the RGCs that were detected. Indeed, some RGCs could not be properly analyzed mostly due to overlapping of dendritic arbors with those of other labeled, neighboring cells. As in the case of the total number of labeled RGCs, also the number of RGCs considered for analysis was higher in the control group than in the STZ group or the STZ+OCT group, but without statistical significance (Supplementary Fig. 4B; Supplementary Tables 2 and 3).

The morphometric analyses did not reveal any statistically significant difference among experimental groups in any of the parameters listed above in the G3/G7, G9, and G13/G14 subtypes. Interestingly, considering only the retinas of control animals and pooling together the morphometric data of the RGC subtypes whose dendritic arbors and/or somata were affected by the STZ and/or the STZ+OCT treatments and those of the RGC subtypes that were unaffected, it appeared that the dendrite area of the unaffected RGCs was significantly smaller (Supplementary Fig. 6). For the RGC subtypes displaying changes in consequence of the treatments, statistically significant differences were found in some parameters and not in others. The following description considers only those parameters in which such significant differences were detected.

In the RGCs belonging to subtype G1, a significant increase of the

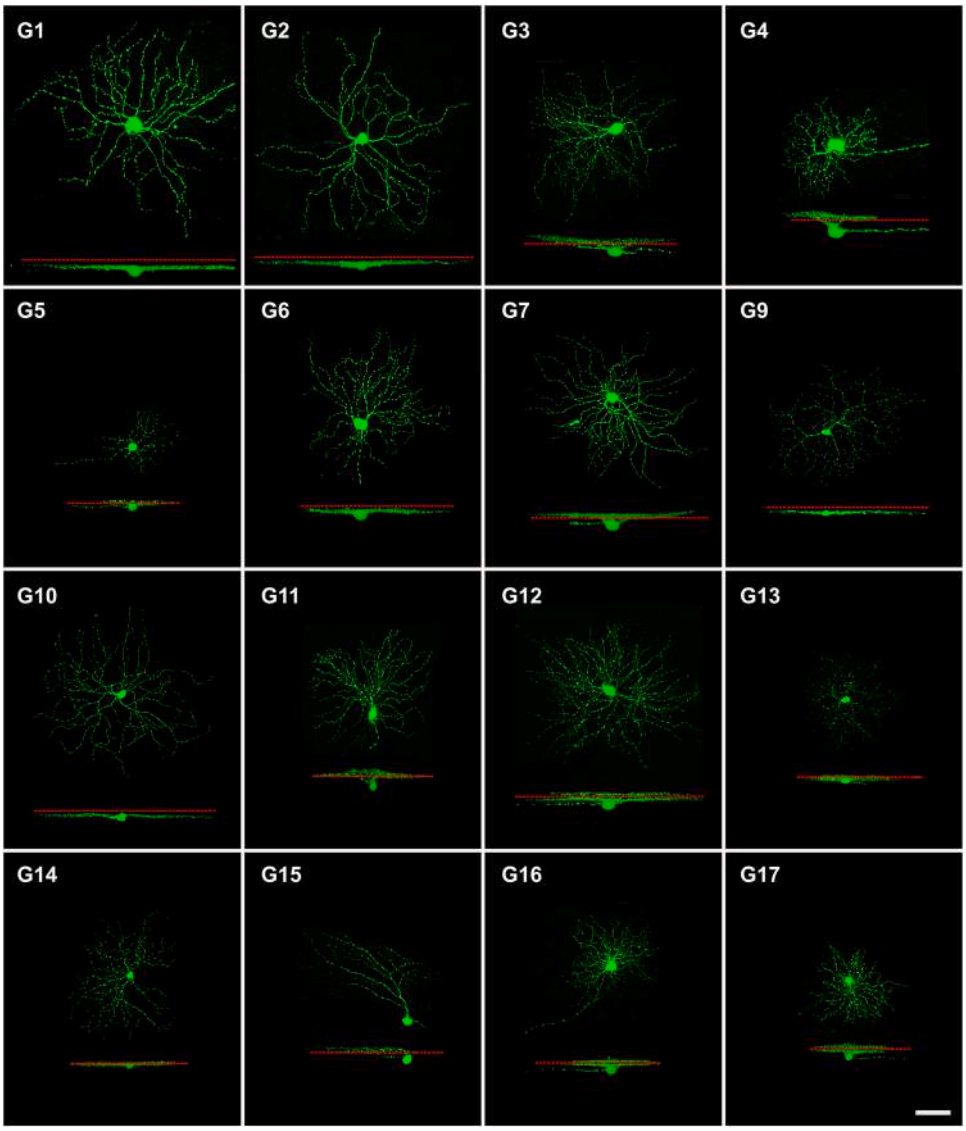

Fig. 4. Representative images of sixteen different RGC subtypes detected in control retinas. Each RGC is shown in whole mount (top part of the panels) and in vertical view after computer rotation (bottom part of the panels). In each panel, the dashed red line indicates the boundary between the OFF (above) and the ON (below) sublaminae of the IPL. The nomenclature of Völgyi et al. [39] was adopted. Scale bar, 50 μm.

soma area was observed in the STZ group, while this effect was abolished in STZ+OCT retinas (Fig. 5A). In addition, the dendrite area was decreased in both STZ and STZ+OCT retinas, with respect to controls, with statistical significance in STZ+OCT (Fig. 5B). In addition, STZ retinas also displayed G1 RGCs with lower numbers of end-point voxels and of junctions, while these decreases were not observed in STZ+OCT retinas (Fig. 5C-D). G1 RGCs displayed some variability in their responses to STZ and to OCT treatments (Fig. 5E-I), but, overall, they reacted to hyperglycemia with increased soma size and with reduced dendrite complexity, and these changes were mostly counteracted by the treatment with OCT. Similarly, in G6 RGCs STZ administration provoked a significant reduction of both average and maximum dendritic branch length, while treatment with OCT resulted in values that were not significantly different from controls (Fig. 6).

Regarding the G2/G10 subtype (Fig. 7), the onset of diabetes promoted an increase of the soma area, while different RGC parameters, including the number of branches, of end-point voxels, of junction voxels, of slab voxels, and of quadruple points were similar in control and in STZ retinas. Of interest, in STZ+OCT retinas these values were significantly decreased vs STZ but were not different from those of controls, suggesting that the treatment with OCT counteracted a tendency to the increment of these parameters in STZ retinas, although with some variability (see Fig. 7G-J).

Similar to G2/G10 RGCs, also those of the G15 subtype displayed alterations towards an increase in a number of parameters following STZ treatment, including dendrite area and number of branches, of end-point voxels, of junctions, of junction voxels, of slab voxels, and of triple and quadruple points (Fig. 8). In most cases, these increases reached statistical significance, while they were abolished in STZ+OCT retinas. Overall, both G2/G10 and G15 RGCs appeared to respond to the onset of diabetes with a trend toward an increased dendrite complexity, while treatment with OCT inhibited these changes.

In the RGCs of the G12 subtype, soma area, dendrite area as well as the number of branches, of end-point voxels, of junctions, of slab voxels, and of triple and quadruple points showed a general tendency to decrease in STZ retinas with respect to controls, without reaching statistical significance in most cases (Fig. 9). However, the notable finding was that statistical significance in these decreases with respect to controls was reached in all parameters after treatment with OCT. Overall, G12 RGCs appeared to be affected by the onset of diabetes only to a

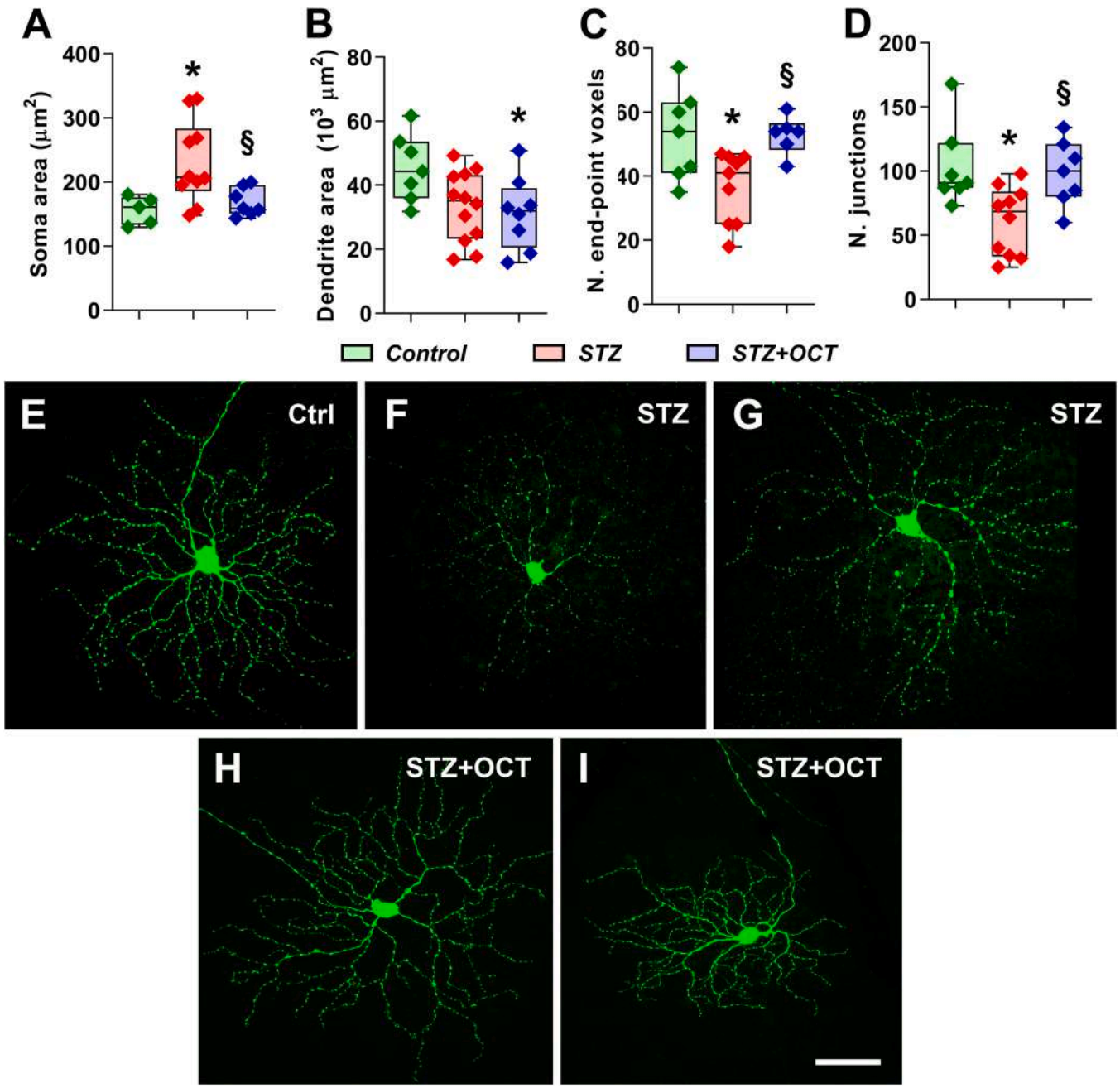

Fig. 5. Morphometric analysis of the RGCs belonging to subtype G1. Box and violin graphs show the values of soma area (A), dendrite area (B), number of end-point voxels (C), and number of junctions (D) recorded in retinas of control, STZ, and STZ+OCT mice. Statistical significance was assessed by one-way ANOVA followed by Tukey's multiple comparison post-hoc test. $5 \leq N \leq 12$. *$p < 0.05$ vs control; §$p < 0.05$ vs STZ. (E) Representative G1 RGC in a control retina. (F) and (G) show G1 RGCs with different degree of damage in STZ retinas. (H) and (I) show G1 RGCs with different degree of damage in STZ+OCT retinas. Scale bar, 50 μm.

limited degree, but the treatment with OCT seemed to exacerbate this response. Similar changes, although limited to the soma size, were detected in G4 and in G16/G17 RGCs, where no appreciable changes could be detected in retinas of STZ mice, while OCT treatment determined a significant decrease of the soma area (Supplementary Fig. 7). All morphometric data are summarized in the graphs of Supplementary Fig. 8 (I-V).

4. Discussion

Although a cohort of diabetic pre-clinical animal models has been established to study visual complications induced by diabetes [40–42] the rodent model of STZ-induced hyperglycemia has been increasingly used during the last 10 years to mimic the human condition of DR as well as possible therapeutic approaches [43]. However, only little information is available on the morpho-functional characteristics of RGCs at very early times after diabetes induction. This knowledge is crucial to understand the primary reactions of retinal neurons to diabetes onset, in order to clarify the link between neuronal changes and microvascular lesions and the utility of early neuroprotective therapies. In the present study, focused on mouse RGCs during the first 2 weeks after STZ treatment, we show that RGCs respond very early to a hyperglycemic state displaying important physiological and structural changes. A treatment with the neuroprotective agent OCT rescues RGC functionality and seems to induce different morphological responses among RGC subtypes.

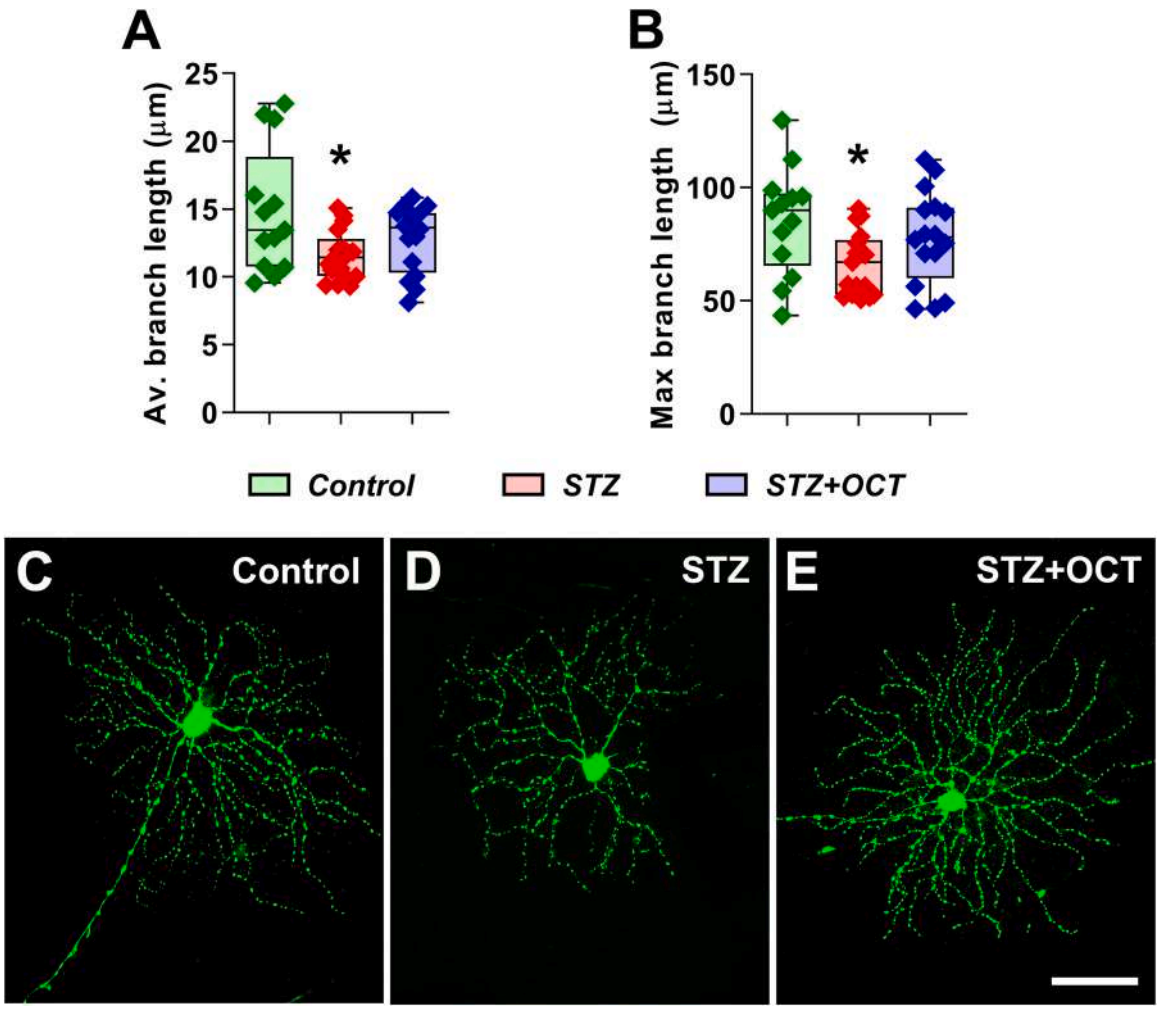

Fig. 6. Morphometric analysis of the RGCs belonging to subtype G6. Box and violin graphs show the values of average branch length (A) and maximum branch length (B) recorded in retinas of control, STZ, and STZ+OCT mice. Statistical significance was assessed by one-way ANOVA followed by Tukey's multiple comparison post-hoc test. $13 \leq N \leq 18$. *$p < 0.05$ vs control. (C), (D), and (E) are representative images of G6 RGCs in control, STZ, and STZ+OCT retinas, respectively. Scale bar, 50 μm.

4.1. OCT rescues RGC function in retinas suffering from diabetes onset

A variety of electroretinographic studies have investigated the functional responses of the retina in diabetic human patients and in rodent models of DR. Together, the data show a progressive deterioration of visual function involving different types of retinal cells, including bipolar cells, amacrine cells, and RGCs [43,44]. However, there are conflicting observations concerning the very early times of DR onset in the mouse model of STZ-induced diabetes. Indeed, at 2 weeks after STZ treatment, some investigations reported reduction of both scERG a- and b-wave [45], while other studies failed to detect such changes [46]. Similarly, at 4 weeks after STZ injection, scERG a- and b-waves were found to decrease in STZ-treated mice [45] or to remain unchanged with respect to control mice [46,47], while no alterations of a-wave and reduction of b-wave were also reported [48]. Interestingly, at 4 weeks after STZ treatment, possible defects in RGC function were suggested by changes in the reduced positive scotopic threshold responses [49] and by PERG impairments [50], while changes in OPs, indicating deficits at the level of synaptic communication in the IPL, were also detected [46,47,51].

Our data show that photoreceptor function is not significantly affected during the first two weeks of diabetes, since both the scERG a-wave and the phERG b-wave, which represent photoreceptor activity [52], have similar amplitudes in all experimental groups. The same can be said for bipolar cells, whose activity is included in the scERG b-wave [52]. In contrast, defects are apparent in the inner retina. Indeed, an analysis of OPs, reflecting the synaptic activity in the IPL [53], revealed changes at 2 weeks after STZ treatment. At the same time, PERG and PhNR amplitudes, two parameters linked to RGC activity [54], are decreased, although statistical significance is reached only for the PERG recordings (this is likely to be due to the fact that PERG is a much more sensitive measure with respect to PhNR [54,55]). In summary, our observations indicate that the first retinal neurons that display functional deficits after diabetes onset are the RGCs, and that these deficits can be appreciated as early as 2 weeks after STZ treatment, that is 11 days after the first recording of a hyperglycemic status, i.e. blood glucose levels higher than 250 mg/dL.

The PERG and PhNR amplitude decreases are counteracted by the intravitreal treatment with the somatostatin analog OCT. Both somatostatin and OCT have been demonstrated to exert important neuroprotective effects in different models of retinal ischemia or DR by inhibiting inflammation, oxidative stress, apoptosis, glutamate release, and formation of advanced glycation end-products, and by increasing autophagy [19–23,56,57]. Our observations clearly indicate that an early neuroprotective intervention may efficiently avoid the appearance of the very first functional alterations due to diabetes.

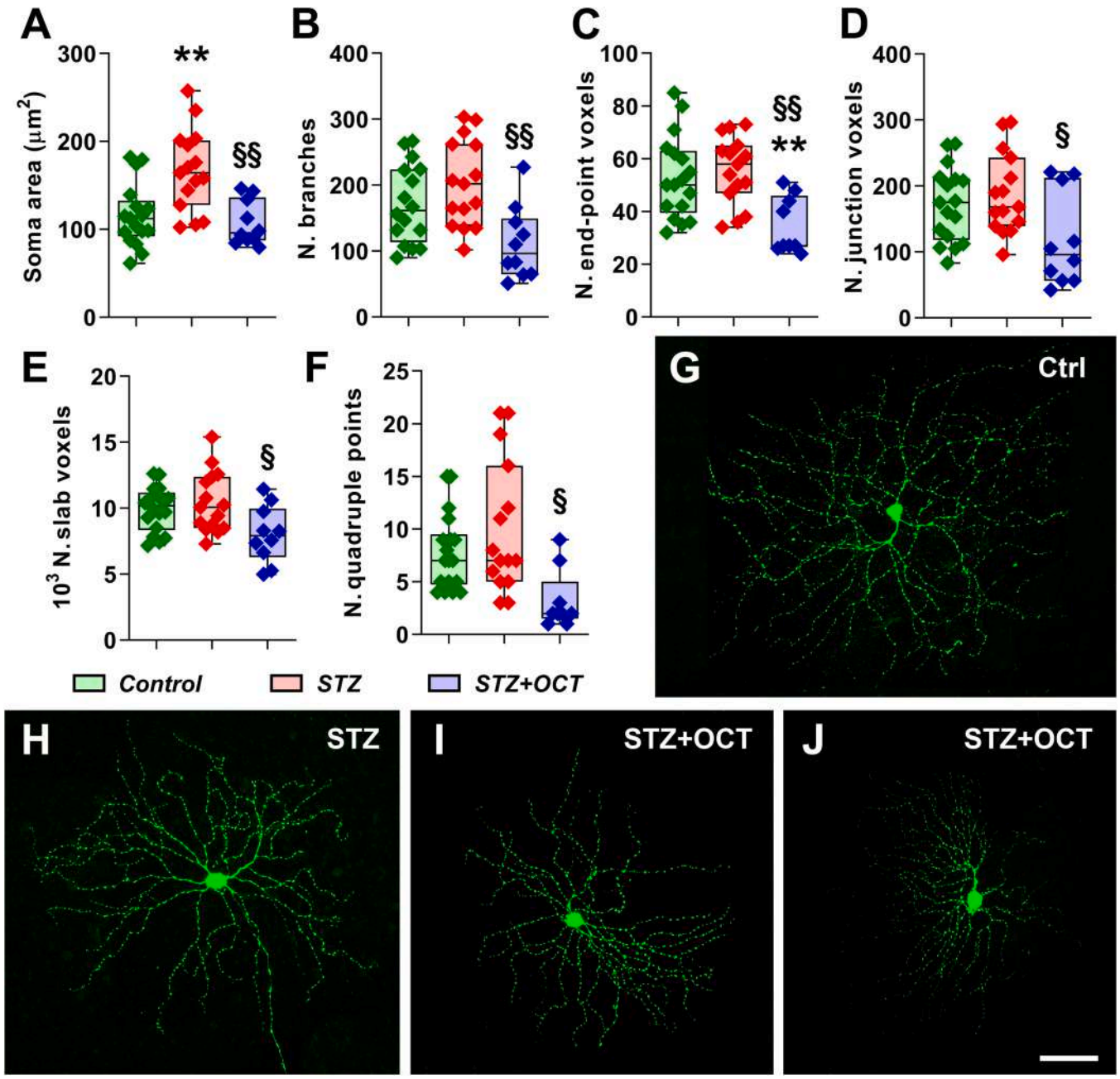

Fig. 7. Morphometric analysis of the RGCs belonging to subtype G2/G10. Box and violin graphs show the values of soma area (A), number of branches (B), number of end-point voxels (C), number of junction voxels (D), number of slab voxels (E), and number of quadruple points (F) recorded in retinas of control, STZ, and STZ+OCT mice. Statistical significance was assessed by one-way ANOVA followed by Tukey's multiple comparison post-hoc test. $10 \leq N \leq 18$. * *$p < 0.01$ vs control; §$p < 0.05$, §§$p < 0.01$ vs STZ. (G) Representative G2/G10 RGC in a control retina. (H) Representative G2/G10 RGC in a STZ retina. (I) and (J) show G2/G10 RGCs with different degree of damage in STZ+OCT retinas. Scale bar, 50 μm.

4.2. RGCs are damaged, but not killed, by diabetes onset

As in the case of functional retinal responses, there are dishomogeneous findings in the literature concerning the presence of apoptotic RGCs in the STZ mouse model up to 2 weeks after STZ treatment. Indeed, some apoptotic RGCs have been reported as early as 4 days [58] and at 2 weeks after STZ treatment [59,60], while no signs of retinopathy have been found using optical coherence tomography at 7 days or at 2 weeks after STZ treatment [45]. A number of studies agree that RGC death is a distinctive feature of the STZ mouse model starting at 4 weeks after STZ treatment, when reduced numbers of RGCs, RGC axon degeneration, and increased presence of apoptotic markers have been reported [15,48,61,62].

With our morphological analyses, we aimed at providing an anatomical basis for the functional changes observed in RGCs at 2 weeks after STZ treatment and for the protective effect afforded by OCT. Two observations may set the frame for discussing these data: first, the number of damaged RGCs increased in the retinas of STZ-injected mice, while OCT treatment reduced this effect; second, no differences in RGC density were observed between the experimental groups, suggesting that, although in principle the presence of some apoptotic RGC cannot be excluded, no significant RGC death was caused by diabetes. Therefore, the observed RGC functional deficits at endpoint are unlikely to be caused by cell loss. This is important, since an early neuroprotective treatment may be effective in rescuing damaged but still alive RGCs, while it could not resuscitate dead cells.

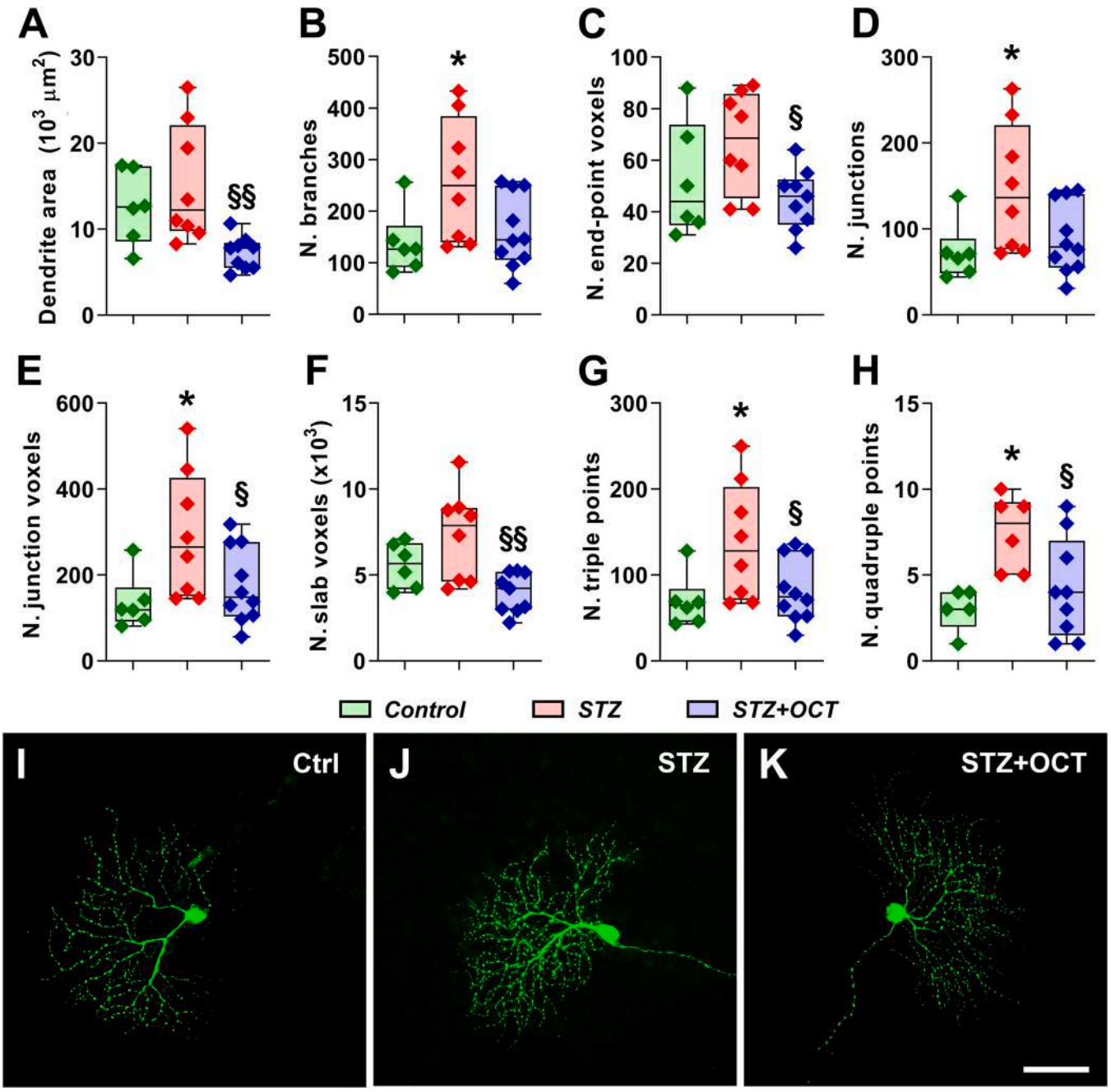

Fig. 8. Morphometric analysis of the RGCs belonging to subtype G15. Box and violin graphs show the values of dendrite area (A), number of branches (B), number of end-point voxels (C), number of junctions (D), number of junction voxels (E), number of slab voxels (F), number of triple points (G), and number of quadruple points (H) recorded in retinas of control, STZ, and STZ+OCT mice. Statistical significance was assessed by one-way ANOVA followed by Tukey's multiple comparison post-hoc test. $5 \leq N \leq 10$. *$p < 0.05$ vs control; $^{\S}p < 0.05$, $^{\S\S}p < 0.01$ vs STZ. (I), (J), and (K) are representative images of G15 RGCs in control, STZ, and STZ+OCT retinas, respectively. Scale bar, 50 µm.

4.3. Diabetes affects some RGC subtypes but not others

Our data are based on the observation of 637 RGCs and on the morphometric analysis of a total of 306 RGCs (Supplementary Tables 2 and 3). Although lower numbers of labeled RGCs were detected in STZ and in STZ+OCT retinas than in control retinas, the differences were not statistically significant. However, the possibility exists that lower numbers of labeled RGCs in STZ- and in STZ+OCT-treated groups may depend on reduced levels of Thy1 expression in stressed RGCs, as observed in retinas of mice subjected to experimental glaucoma or to optic nerve crush [63].

Our data indicate that the susceptibility to STZ is not strictly associated to ON-type or OFF-type RGCs, since RGCs of both types resulted to be affected or unaffected by diabetes. Instead, our observations suggest that RGCs with smaller dendritic arbors are less susceptible to the effects induced by STZ treatment. This result reminds of observations in glaucomatous monkey and cat retinas, in which large-sized RGCs were more seriously damaged than smaller RGCs [64,65]. Large RGCs are likely to be more susceptible to damage due to their smaller surface-to-volume ratio and higher demand of energy and oxygen. The possibility also exists that large RGCs are more sensitive than small RGCs to glutamate excitotoxicity, a condition that is present in the diabetic retina [66], due to the higher number of glutamate receptors expressed on their dendrites, although reduction of dendritic tree size did not

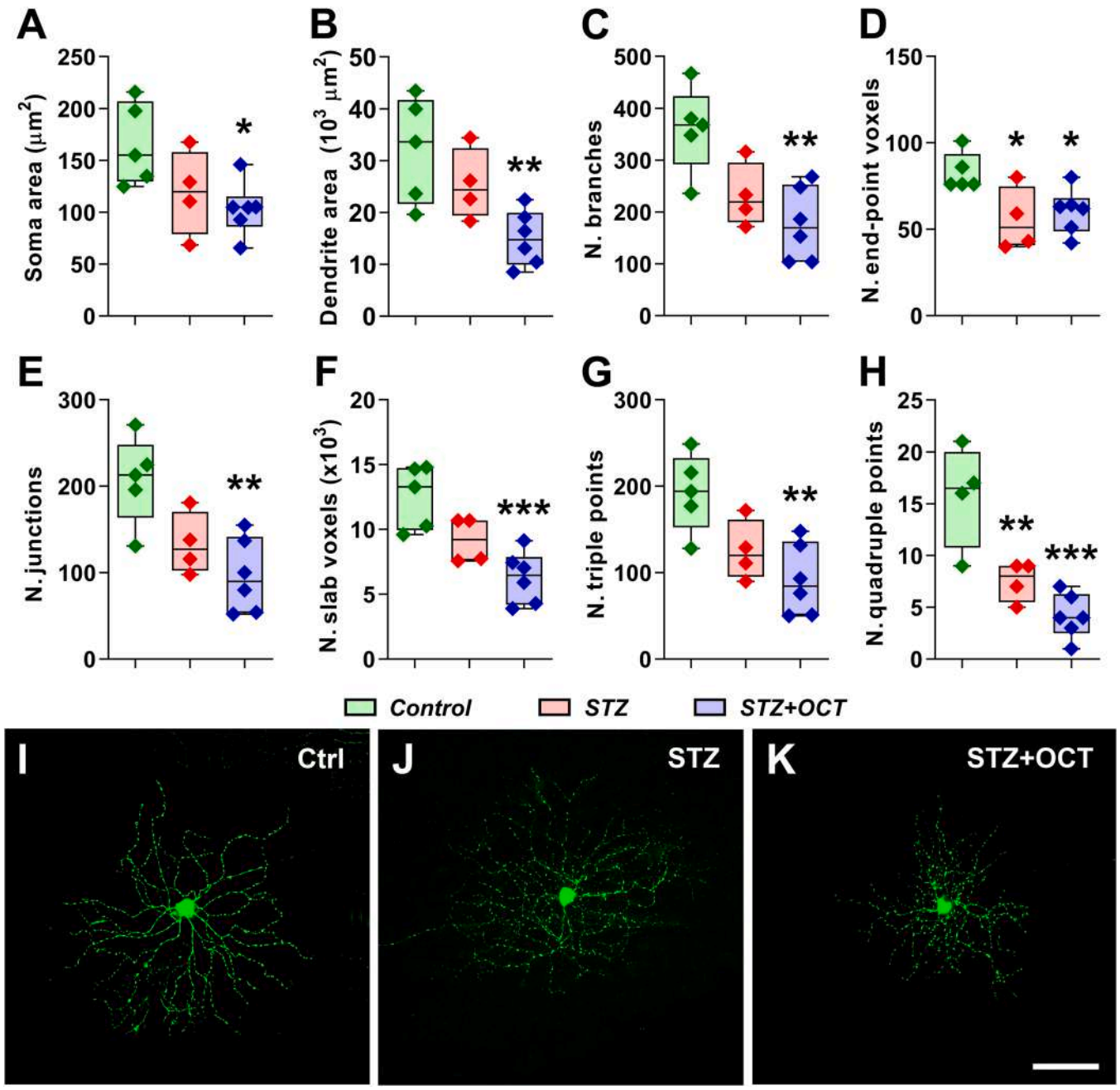

Fig. 9. Morphometric analysis of the RGCs belonging to subtype G12. Box and violin graphs show the values of soma area (A), dendrite area (B), number of branches (C), number of end-point voxels (D), number of junctions (E), number of slab voxels (F), number of triple points (G), and number of quadruple points (H) recorded in retinas of control, STZ, and STZ+OCT mice. Statistical significance was assessed by one-way ANOVA followed by Tukey's multiple comparison post-hoc test. $4 \leq N \leq 6$. *$p < 0.05$, * *$p < 0.01$, * **$p < 0.001$ vs control. (I), (J), and (K) are representative images of G12 RGCs in control, STZ, and STZ+OCT retinas, respectively. Scale bar, 50 μm.

protect cerebellar Purkinje cells from glutamate-induced damage [67].

Concerning morphological changes of RGCs, quantitative studies on RGC dendrite morphology in DR are not numerous and they have been reviewed recently [10,68]. Although scarce, these data suggest that different subtypes of RGCs are likely to respond in different ways to the diabetic insult. To our knowledge, the present study is the first investigation providing detailed information on the responses to a brief period of hyperglycemia by specific morphologically-identified RGC subtypes.

4.4. OCT recovers some RGC subtypes and induces adaptive changes in others

In G1 RGCs, OCT induced a decrease of the soma size, which was increased in STZ mice, and it also recovered parameters of dendrite complexity (although not the dendrite area). In the same way, OCT protected G6 RGCs from a STZ-induced decrease of dendritic branch length. A similar effect, although of opposite sign, was observed in G2/G10 and in G15 RGCs, where dendrite area and dendrite complexity tended to increase in STZ mice, while this effect was counteracted by OCT. In contrast, an unexpected effect of OCT, which seemed to reinforce the changes caused by STZ-induced diabetes, was evident in G12

RGCs, where all the parameters, including soma area and a number of dendrite characteristics, tended to decrease in STZ mice and they were even more drastically decreased by OCT. Similar effects, although only affecting the soma size, were also observed in G4 and in G16/G17 RGCs. Overall, it seems that, besides the RGC subtypes that are unaffected by diabetes, there is a group of RGCs (Group 1) that are rescued by OCT (G1, G2/G10, G6, and G15) and another group of RGCs (Group 2) in which OCT seems to worsen the effect of diabetes (G12, G4, and G16/G17). Considering that OCT preserves ERG properties, our results indicate that, while in some RGCs OCT affords full protection from hyperglycemia-induced damage, in others it may induce changes that promote adaptation to the increased metabolic stress and may allow the RGC to maintain an almost unaltered functional activity. These changes are likely to include elimination of cellular components to reduce energy expenditure through autophagic processes. This is in line with our recent findings obtained with *ex vivo* retinal explants showing that an OCT-induced increase of autophagy may protect the retinal tissue by high glucose-induced damage [20].

Of interest, the ON, OFF, or ON/OFF characteristics of Group 1 and Group 2 RGCs may explain the dual effects of OCT. Most of the RGCs in Group 1 are ON-type RGCs (with the exception of the G15, OFF-type RGCs), while most of the RGCs in Group 2 are ON/OFF type RGCs (with the exception of the G4, OFF-type RGCs). Therefore, the possibility exists that the detrimental responses characterizing the RGCs in Group 2 are associated to an ON/OFF profile. Indeed, these RGCs have two dendritic arbors (one in the proximal and the other in the distal IPL sublamina), and the particularly high degree of complexity of their dendritic arborizations may affect the response to OCT. In this respect, after pooling together the morphometric data of the two groups of RGCs in control retinas, it appears that the RGCs in Group 2 have higher number of branches with shorter length and more junctions (Fig. 10), indicating greater density and complexity of their arborizations. These observations suggest that a simplification of the dendritic tree in some RGC subtypes is likely to result in a metabolic advantage that may sustain RGC homeostasis.

The coupling of different RGC subtypes with other RGCs or with amacrine cells also deserves to be considered. Indeed, according to Völgyi et al. [39], different RGC subtypes establish different coupling patterns through gap junctions with amacrine cells (heterologous coupling) and / or with other RGCs (homologous coupling). The RGC subtypes of Group 1, in which OCT counteracts the effects of diabetes onset, are all characterized by heterologous coupling, with G10 RGCs also showing some degree of homologous coupling. In contrast, among the RGCs of Group 2, in which OCT induces an apparent worsening, there are some establishing only homologous coupling (G16 and G17), a subtype in which no signs of coupling were observed (G12), while only the G4 RGCs displayed heterologous coupling [39] (Supplementary Table 4). Thus, it seems that a heterologous coupling with a certain number of amacrine cells is a condition that may allow a RGC to obtain full protection by OCT. Gap junctions are highly represented in retinal circuits, where they subserve a variety of functions [69]. In particular, coupling between RGCs and amacrine cells may result in enhanced inhibition within RGC circuits [70], or may be implicated in global object perception [71]. In our context, gap junctions should be considered as important contributors to neuronal death and survival. Indeed, propagation of chemical signals through gap junctions may expand cell death to the whole group of coupled cells or may favor their survival. For instance, "pro-survival" signals are likely to include ATP and free radical scavengers [72]. Additionally, heterologous coupling between RGCs and amacrine cells may contribute to spontaneous waves of electric activity, which play a role during retinal development and positively affect stressed neurons in the diseased retina [73].

Under a mechanistic point of view, it is known that OCT preferentially binds somatostatin subtype receptor (sst) 2 and 5 and has moderate affinity for sst3 [30]. In the mouse retina, sst5 are expressed by RGCs [74], while sst2 has been detected in rod bipolar cells and in selected populations of amacrine cells [75]. Therefore, OCT may protect RGCs from hyperglycemia-induced damage acting directly on sst5 expressed by them. Accordingly, the selective activation of sst5 has been found to be protective for RGCs in experimental glaucoma [76]. In addition, OCT coupling to sst2 has been shown to inhibit glutamate release from mouse bipolar cells [77], suggesting that OCT may save RGCs by decreasing excitotoxicity, which is likely to affect RGCs in diabetic retinas [78]. Finally, we cannot exclude that the activation of sst2 expressed by amacrine cells might favor the delivery of pro-survival signals to RGCs through heterologous coupling.

5. Conclusions

The present study reveals a very early response of RGCs to the onset of diabetes and indicate that similar changes are likely to characterize the initial phases of DR. This response involves the appearance of functional deficits and abnormalities in morphometric parameters of most RGC subtypes, but not overt cell death. A pharmacologic treatment with the neuroprotective somatostatin analog OCT preserves RGC functionality and induces adaptive changes that are different for specific

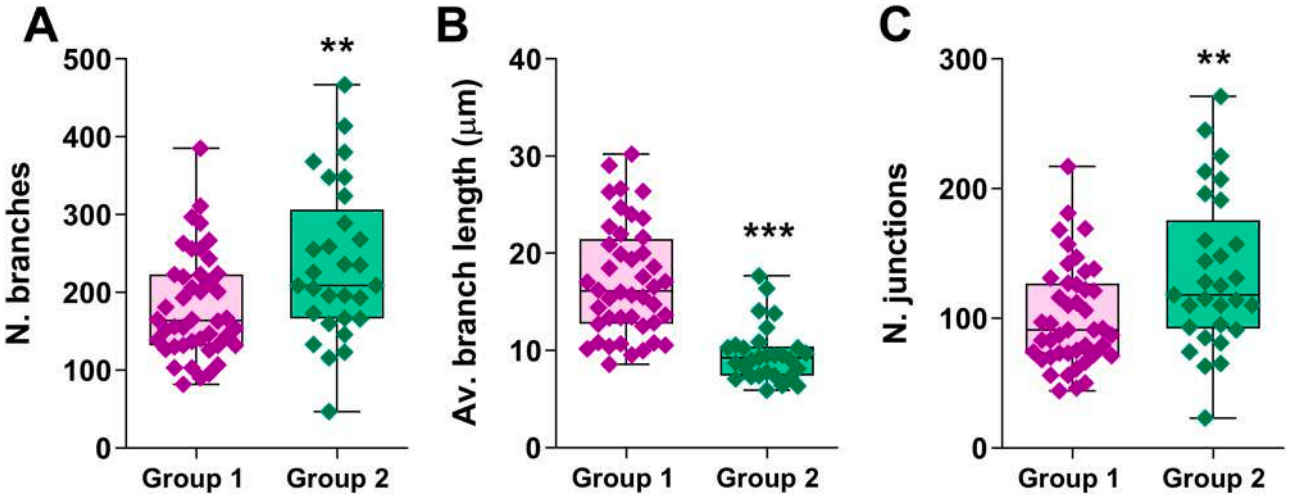

Fig. 10. Comparison of three different parameters indicating overall complexity of the dendritic arborization, as measured in control retinas, between the RGCs that were rescued by OCT treatment (including G1, G6, G2/G10, and G15 RGCs; Group 1) and those in which OCT seemed to worsen the effects of diabetes (including, G12, G4, and G16/G17 RGCs; Group 2). Student's *t*-test. $44 \leq N \leq 29$. * *$p < 0.01$, * **$p < 0.001$ vs Group 1.

RGC subtypes. It appears that large RGCs are mostly affected by diabetes and respond to OCT treatment, while those with smaller dendritic arborizations are less involved. Interestingly, depending on the complexity of the dendritic tree and/or the degree of heterologous coupling of RGCs, OCT may completely rescue RGC morphometric parameters or induce further reductions of dendrite branching or of soma size. Although different, both effects of OCT are likely to contribute to the maintenance of RGC functionality in the presence of diabetes-induced metabolic stress. These results highlight the importance of pharmacologic interventions to protect retinal neurons in very early phases of the disease, when apoptotic phenomena have not yet started and RGC morphometric characteristics can be preserved or adjusted to maintain function.

CRediT authorship contribution statement

DC and GC designed the study. RA, DC, and GC wrote the manuscript. EC collected the confocal RGC images and made a first morphometric analysis. GC completed the morphometric analysis. RA performed the ERG experiments and analyzed the data. MC and MDM collaborated to data analysis and preparation of manuscript. MC, MDM, DC, and GC contributed reagents and materials. All authors approved the manuscript.

Declaration of Competing Interest

The authors declare that they have no known competing financial interests or personal relationships that could have appeared to influence the work reported in this paper.

Data Availability

Data will be made available on request.

Acknowledgements

This study was supported by funding from Italian Ministry of University and Research (PRIN2017 to DC) and by Fondazione Cassa di Risparmio di Firenze (to MDM and GC). We thank Dr. Maria Grazia Rossino for her help in the initial phases of this study.

Appendix A. Supporting information

Supplementary data associated with this article can be found in the online version at doi:10.1016/j.phrs.2022.106516.

References

[1] U.S. Kim, O.A. Mahroo, J.D. Mollon, P. Yu-Wai-Man, Retinal ganglion cells-diversity of cell types and clinical relevance (eCollection), Front Neurol. 2021 (12) (2021), https://doi.org/10.3389/fneur.2021.661938.
[2] V. Porciatti, T.H. Chou, Modeling retinal ganglion cell dysfunction in optic neuropathies, Cells (2021) 10, https://doi.org/10.3390/cells10061398.
[3] L.K. Wareham, M.L. Risner, D.J. Calkins, Protect, repair, and regenerate: towards restoring vision in glaucoma, Curr. Ophthalmol. Rep. 8 (2020) 301–310, https://doi.org/10.1007/s40135-020-00259-5.
[4] E. Yenice, A. Şengün, G. Soyugelen Demirok, E. Turaçlı, Ganglion cell complex thickness in nonexudative age-related macular degeneration, Eye 29 (2015) 1076–1080, https://doi.org/10.1038/eye.2015.86.
[5] Y.A. Ito, A. Di Polo, Mitochondrial dynamics, transport, and quality control: a bottleneck for retinal ganglion cell viability in optic neuropathies, Mitochondrion 36 (2017) 186–192, https://doi.org/10.1016/j.mito.2017.08.014.
[6] C. Hernández, M. Dal Monte, R. Simó, G. Casini, Neuroprotection as a therapeutic target for diabetic retinopathy, J. Diabetes Res 9508541 (2016) 31. DOI:1155/2016/9508541.
[7] E.H. Sohn, H.W. van Dijk, C. Jiao, P.H. Kok, W. Jeong, N. Demirkaya, et al., Retinal neurodegeneration may precede microvascular changes characteristic of diabetic retinopathy in diabetes mellitus, Proc. Natl. Acad. Sci. USA 113 (2016) 25, https://doi.org/10.1073/pnas.1522014113.
[8] J. Lechner, O.E. O'Leary, A.W. Stitt, The pathology associated with diabetic retinopathy, Vis. Res. 139 (2017) 7–14, https://doi.org/10.1016/j.visres.2017.04.003.
[9] A.K. Lai, A.C. Lo, Animal models of diabetic retinopathy: summary and comparison, J. Diabetes Res. 106594 (2013) 27. DOI:1155/2013/106594.
[10] E. Catalani, D. Cervia, Diabetic retinopathy: a matter of retinal ganglion cell homeostasis, Neural Regen. Res 15 (2020) 1253–1254, https://doi.org/10.4103/1673-5374.272577.
[11] Y. Qin, G. Xu, W. Wang, Dendritic abnormalities in retinal ganglion cells of three-month diabetic rats, Curr. Eye Res 31 (2006) 967–974, https://doi.org/10.1080/02713680600987674.
[12] M.J. Gastinger, A.R. Kunselman, E.E. Conboy, S.K. Bronson, A.J. Barber, Dendrite remodeling and other abnormalities in the retinal ganglion cells of Ins2 Akita diabetic mice, Invest Ophthalmol. Vis. Sci. 49 (2008) 2635–2642, https://doi.org/10.1167/iovs.07-0683.
[13] B. Meyer-Rüsenberg, M. Pavlidis, T. Stupp, S. Thanos, Pathological changes in human retinal ganglion cells associated with diabetic and hypertensive retinopathy, Graefes Arch. Clin. Exp. Ophthalmol. 245 (2007) 1009–1018, https://doi.org/10.1007/s00417-006-0489-x.
[14] R.Z. Cui, L. Wang, S.N. Qiao, Y.C. Wang, X. Wang, F. Yuan, et al., ON-type retinal ganglion cells are preferentially affected in STZ-induced diabetic mice, Invest Ophthalmol. Vis. Sci. 60 (2019) 1644–1656, https://doi.org/10.1167/iovs.18-26359.
[15] J. Sergeys, I. Etienne, I. Van Hove, E. Lefevere, I. Stalmans, J.H.M. Feyen, et al., Longitudinal in vivo characterization of the streptozotocin-induced diabetic mouse model: focus on early inner retinal responses, Invest Ophthalmol. Vis. Sci. 60 (2019) 807–822, https://doi.org/10.1167/iovs.18-25372.
[16] M.G. Rossino, M. Dal Monte, G. Casini, Relationships between neurodegeneration and vascular damage in diabetic retinopathy (eCollection), Front Neurosci. (2019) 13, https://doi.org/10.3389/fnins.2019.01172.
[17] M.G. Rossino, M. Lulli, R. Amato, M. Cammalleri, M.D. Monte, G. Casini, Oxidative stress induces a VEGF autocrine loop in the retina: relevance for diabetic retinopathy, Cells (2020) 9, https://doi.org/10.3390/cells9061452.
[18] D. Cervia, E. Catalani, G. Casini, Neuroprotective peptides in retinal disease, J. Clin. Med (2019) 8, https://doi.org/10.3390/jcm8081146.
[19] R. Amato, M. Biagioni, M. Cammalleri, M. Dal Monte, G. Casini, VEGF as a survival factor in ex vivo models of early diabetic retinopathy, Invest Ophthalmol. Vis. Sci. 57 (2016) 3066–3076, https://doi.org/10.1167/iovs.16-19285.
[20] R. Amato, E. Catalani, M. Dal Monte, M. Cammalleri, I. Di Renzo, C. Perrotta, et al., Autophagy-mediated neuroprotection induced by octreotide in an ex vivo model of early diabetic retinopathy, Pharmacol. Res. 128 (2018) 167–178, https://doi.org/10.1016/j.phrs.2017.09.022.
[21] R. Amato, M. Giannaccini, M. Dal Monte, M. Cammalleri, A. Pini, V. Raffa, et al., Association of the somatostatin analog octreotide with magnetic nanoparticles for intraocular delivery: a possible approach for the treatment of diabetic retinopathy (eCollection), Front Bioeng. Biotechnol. 2020 (2020) 8, https://doi.org/10.3389/fbioe.2020.00144.
[22] D. Cervia, E. Catalani, M. Dal Monte, G. Casini, Vascular endothelial growth factor in the ischemic retina and its regulation by somatostatin, J. Neurochem. 120 (2012) 818–829, https://doi.org/10.1111/j.1471-4159.2011.07622.x.
[23] D. Cervia, D. Martini, C. Ristori, E. Catalani, A.M. Timperio, P. Bagnoli, et al., Modulation of the neuronal response to ischaemia by somatostatin analogues in wild-type and knock-out mouse retinas, J. Neurochem. 106 (2008) 2224–2235, https://doi.org/10.1111/j.1471-4159.2008.05556.x.
[24] M. Gomes-Porras, J. Cárdenas-Salas, C. Álvarez-Escolá, Somatostatin analogs in clinical practice: a review, Int J. Mol. Sci. (2020) 21, https://doi.org/10.3390/ijms21051682.
[25] G. Feng, R.H. Mellor, M. Bernstein, C. Keller-Peck, Q.T. Nguyen, M. Wallace, et al., Imaging neuronal subsets in transgenic mice expressing multiple spectral variants of GFP, Neuron 28 (2000) 41–51, https://doi.org/10.1016/s0896-6273(00)00084-2.
[26] F. Mazzoni, E. Novelli, E. Strettoi, Retinal ganglion cells survive and maintain normal dendritic morphology in a mouse model of inherited photoreceptor degeneration, J. Neurosci. 28 (2008) 14282–14292.
[27] D. Cervia, D. Fehlmann, D. Hoyer, Native somatostatin sst2 and sst5 receptors functionally coupled to Gi/o-protein, but not to the serum response element in AtT-20 mouse tumour corticotrophs, Naunyn Schmiede Arch. Pharmacol. 367 (2003) 578–587, https://doi.org/10.1007/s00210-003-0752-1.
[28] D. Cervia, S. Fiorini, B. Pavan, C. Biondi, P. Bagnoli, Somatostatin (SRIF) modulates distinct signaling pathways in rat pituitary tumor cells; negative coupling of SRIF receptor subtypes 1 and 2 to arachidonic acid release, Naunyn Schmiede Arch. Pharm. 365 (2002) 200–209, https://doi.org/10.1007/s00210-001-0509-7.
[29] D. Cervia, P. Zizzari, B. Pavan, E. Schuepbach, D. Langenegger, D. Hoyer, et al., Biological activity of somatostatin receptors in GC rat tumour somatotrophs: evidence with sst1-sst5 receptor-selective nonpeptidyl agonists, Neuropharmacology 44 (2003) 672–685, https://doi.org/10.1016/s0028-3908(03)00031-5.
[30] C. Bruns, F. Raulf, D. Hoyer, J. Schloos, H. Lübbert, G. Weckbecker, Binding properties of somatostatin receptor subtypes, Metabolism 45 (1996) 17–20, https://doi.org/10.1016/s0026-0495(96)90072-4.
[31] B. Pavan, S. Fiorini, M. Dal Monte, L. Lunghi, C. Biondi, P. Bagnoli, et al., Somatostatin coupling to adenylyl cyclase activity in the mouse retina, Naunyn Schmiede Arch. Pharm. 370 (2004) 91–98, https://doi.org/10.1007/s00210-004-0950-5.

[32] A. D'Alessandro, D. Cervia, E. Catalani, F. Gevi, L. Zolla, G. Casini, Protective effects of the neuropeptides PACAP, substance P and the somatostatin analogue octreotide in retinal ischemia: a metabolomic analysis, Mol. Biosyst. 10 (2014) 1290–1304, https://doi.org/10.1039/c3mb70362b.
[33] Robson A.G., Frishman L.J., Grigg J., Hamilton R., Jeffrey B.G., Kondo M., et al. ISCEV Standard for full-field clinical electroretinography (2022 update). Doc Ophthalmol 2022;144:165–77. DOI.
[34] A.R. Rodriguez, L.P. de Sevilla Müller, N.C. Brecha, The RNA binding protein RBPMS is a selective marker of ganglion cells in the mammalian retina, J. Comp. Neurol. 522 (2014) 1411–1443, https://doi.org/10.1002/cne.23521.
[35] W. Sun, N. Li, S. He, Large-scale morphological survey of mouse retinal ganglion cells, J. Comp. Neurol. 451 (2002) 115–126, https://doi.org/10.1002/cne.10323.
[36] T.C. Badea, J. Nathans, Quantitative analysis of neuronal morphologies in the mouse retina visualized by using a genetically directed reporter, J. Comp. Neurol. 480 (2004) 331–351. DOI:doi: 10.1002/cne.20304.
[37] J.H. Kong, D.R. Fish, R.L. Rockhill, R.H. Masland, Diversity of ganglion cells in the mouse retina: unsupervised morphological classification and its limits, J. Comp. Neurol. 489 (2005) 293–310, https://doi.org/10.1002/cne.20631.
[38] J. Coombs, D. van der List, G.Y. Wang, L.M. Chalupa, Morphological properties of mouse retinal ganglion cells, Neuroscience 140 (2006) 123–136, https://doi.org/10.1016/j.neuroscience.2006.02.079.
[39] B. Völgyi, S. Chheda, S.A. Bloomfield, Tracer coupling patterns of the ganglion cell subtypes in the mouse retina, J. Comp. Neurol. 512 (2009) 664–687, https://doi.org/10.1002/cne.21912.
[40] E. Catalani, F. Silvestri, S. Bongiorni, A.R. Taddei, G. Fanelli, S. Rinalducci, et al., Retinal damage in a new model of hyperglycemia induced by high-sucrose diets, Pharmacol. Res. 166 (2021) 11, https://doi.org/10.1016/j.phrs.2021.105488.
[41] P.M. Pitale, M.S. Gorbatyuk, Diabetic retinopathy: from animal models to cellular signaling, Int J. Mol. Sci. (2022) 23. DOI:0.3390/ijms23031487.
[42] J. Quiroz, A. Yazdanyar, Animal models of diabetic retinopathy, Ann. Transl. Med. 9 (2021) 20–6737, https://doi.org/10.21037/atm-20-6737.
[43] I. Lelyte, Z. Ahmed, S. Kaja, G. Kalesnykas, Structure-function relationships in the rodent streptozotocin-induced model for diabetic retinopathy: a systematic review, J. Ocul. Pharmacol. Ther. 38 (2022) 271–286, https://doi.org/10.1089/jop.2021.0128.
[44] E.D. Eggers, T.A. Carreon, The effects of early diabetes on inner retinal neurons, Vis. Neurosci. (2020) 16, https://doi.org/10.1017/S095252382000005X.
[45] I.S. Samuels, B.A. Bell, A. Pereira, J. Saxon, N.S. Peachey, Early retinal pigment epithelium dysfunction is concomitant with hyperglycemia in mouse models of type 1 and type 2 diabetes, J. Neurophysiol. 113 (2015) 1085–1099, https://doi.org/10.1152/jn.00761.2014.
[46] M.J. Tarchick, A.H. Cutler, T.D. Trobenter, M.R. Kozlowski, E.R. Makowski, N. Holoman, et al., Endogenous insulin signaling in the RPE contributes to the maintenance of rod photoreceptor function in diabetes, Exp. Eye Res. 180 (2019) 63–74, https://doi.org/10.1016/j.exer.2018.11.020.
[47] M.K. Kim, M.H. Aung, L. Mees, D.E. Olson, N. Pozdeyev, P.M. Iuvone, et al., Dopamine deficiency mediates early rod-driven inner retinal dysfunction in diabetic mice, Invest Ophthalmol. Vis. Sci. 59 (2018) 572–581, https://doi.org/10.1167/iovs.17-22692.
[48] W.P. Miller, C. Yang, M.L. Mihailescu, J.A. Moore, W. Dai, A.J. Barber, et al., Deletion of the Akt/mTORC1 repressor REDD1 prevents visual dysfunction in a rodent model of type 1 diabetes, Diabetes 67 (2018) 110–119, https://doi.org/10.2337/db17-0728.
[49] F. Liu, A.B. Saul, P. Pichavaram, Z. Xu, M. Rudraraju, P.R. Somanath, et al., Pharmacological inhibition of spermine oxidase reduces neurodegeneration and improves retinal function in diabetic mice, J. Clin. Med. (2020) 9, https://doi.org/10.3390/jcm9020340.
[50] D. Yuan, Y. Xu, H. Hang, X. Liu, X. Chen, P. Xie, et al., Edaravone protect against retinal damage in streptozotocin-induced diabetic mice (eCollection), PLoS One 2014 (2014) 9, https://doi.org/10.1371/journal.pone.0099219.
[51] M. Sasaki, Y. Ozawa, T. Kurihara, S. Kubota, K. Yuki, K. Noda, et al., Neurodegenerative influence of oxidative stress in the retina of a murine model of diabetes, Diabetologia 53 (2010) 971–979, https://doi.org/10.1007/s00125-009-1655-6.
[52] L.H. Pinto, B. Invergo, K. Shimomura, J.S. Takahashi, J.B. Troy, Interpretation of the mouse electroretinogram, Doc. Ophthalmol. 115 (2007) 127–136.
[53] L. Wachtmeister, Oscillatory potentials in the retina: what do they reveal, Prog. Retin Eye Res. 17 (1998) 485–521.
[54] V. Porciatti, Electrophysiological assessment of retinal ganglion cell function, Exp. Eye Res. 141 (2015) 164–170, https://doi.org/10.1016/j.exer.2015.05.008.
[55] Y. Liu, C.M. McDowell, Z. Zhang, H.E. Tebow, R.J. Wordinger, A.F. Clark, Monitoring retinal morphologic and functional changes in mice following optic nerve crush, Invest Ophthalmol. Vis. Sci. 55 (2014) 3766–3774.
[56] C. Hernández, A.I. Arroba, P. Bogdanov, H. Ramos, O. Simó-Servat, R. Simó, et al., Effect of topical administration of somatostatin on retinal inflammation and neurodegeneration in an experimental model of diabetes, J. Clin. Med (2020) 9, https://doi.org/10.3390/jcm9082579.
[57] C. Hernández, O. Simó-Servat, R. Simó, Somatostatin and diabetic retinopathy: current concepts and new therapeutic perspectives, Endocrine 46 (2014) 209–214, https://doi.org/10.1007/s12020-014-0232-z.
[58] Adhi M., Cashman S.M., Kumar-Singh R.. Adeno-associated virus mediated delivery of a non-membrane targeted human soluble CD59 attenuates some aspects of diabetic retinopathy in mice. PLoS One 2013;8. DOI:doi: 10.1371/journal.pone.0079661. eCollection 2013.
[59] R.A. Feit-Leichman, R. Kinouchi, M. Takeda, Z. Fan, S. Mohr, T.S. Kern, et al., Vascular damage in a mouse model of diabetic retinopathy: relation to neuronal and glial changes, Invest Ophthalmol. Vis. Sci. 46 (2005) 4281–4287, https://doi.org/10.1167/iovs.04-1361.
[60] P.M. Martin, P. Roon, T.K. Van Ells, V. Ganapathy, S.B. Smith, Death of retinal neurons in streptozotocin-induced diabetic mice, Invest Ophthalmol. Vis. Sci. 45 (2004) 3330–3336, https://doi.org/10.1167/iovs.04-0247.
[61] A.Y. Shanab, T. Nakazawa, M. Ryu, Y. Tanaka, N. Himori, K. Taguchi, et al., Metabolic stress response implicated in diabetic retinopathy: the role of calpain, and the therapeutic impact of calpain inhibitor, Neurobiol. Dis. 48 (2012) 556–567, https://doi.org/10.1016/j.nbd.2012.07.025.
[62] S.B. Madrakhimov, J.Y. Yang, J.H. Kim, J.W. Han, T.K. Park, mTOR-dependent dysregulation of autophagy contributes to the retinal ganglion cell loss in streptozotocin-induced diabetic retinopathy, Cell Commun. Signal 19 (2021) 020–00698, https://doi.org/10.1186/s12964-4.
[63] W. Huang, J. Fileta, Y. Guo, C.L. Grosskreutz, Downregulation of Thy1 in retinal ganglion cells in experimental glaucoma, Curr. Eye Res 31 (2006) 265–271.
[64] T. Shou, J. Liu, W. Wang, Y. Zhou, K. Zhao, Differential dendritic shrinkage of alpha and beta retinal ganglion cells in cats with chronic glaucoma, Invest Ophthalmol. Vis. Sci. 44 (2003) 3005–3010.
[65] Y. Glovinsky, H.A. Quigley, G.R. Dunkelberger, Retinal ganglion cell loss is size dependent in experimental glaucoma, Investig. Ophthalmol. Vis. Sci. 32 (1991) 484–491.
[66] K.D. Rolev, X.S. Shu, Y. Ying, Targeted pharmacotherapy against neurodegeneration and neuroinflammation in early diabetic retinopathy, Neuropharmacology 187 (2021) 12.
[67] O.S. Gugger, J.P. Kapfhammer, Reduced size of the dendritic tree does not protect Purkinje cells from excitotoxic death, J. Neurosci. Res 88 (2010) 774–783.
[68] A.J. Barber, B. Baccouche, Neurodegeneration in diabetic retinopathy: potential for novel therapies (Epub), Vis. Res. 139 (2017) 82–92, https://doi.org/10.1016/j.visres.2017.06.014.
[69] Trenholm S., Awatramani G.B. Myriad roles for gap junctions in retinal circuits. In: Kolb H., Fernandez E., Nelson R., editors. Webvision: The Organization of the Retina and Visual System [Internet]. Salt Lake City (UT): University of Utah Health Sciences Center; 2019.
[70] R.E. Marc, C.L. Sigulinsky, R.L. Pfeiffer, D. Emrich, J.R. Anderson, B.W. Jones, Heterocellular coupling between amacrine cells and ganglion cells (eCollection), Front Neural Circuits (2018) 12, https://doi.org/10.3389/fncir.2018.00090.
[71] K. Roy, S. Kumar, S.A. Bloomfield, Gap junctional coupling between retinal amacrine and ganglion cells underlies coherent activity integral to global object perception, Proc. Natl. Acad. Sci. USA 114 (2017) E10484–E10493, https://doi.org/10.1073/pnas.1708261114.
[72] A.B. Belousov, J.D. Fontes, M. Freitas-Andrade, C.C. Naus, Gap junctions and hemichannels: communicating cell death in neurodevelopment and disease, BMC Cell Biol. 18 (2017) 016–0120, https://doi.org/10.1186/s12860-x.
[73] G. Szarka, M. Balogh, Á.J. Tengölics, A. Ganczer, B. Völgyi, T. Kovács-Öller, The role of gap junctions in cell death and neuromodulation in the retina, Neural Regen. Res 16 (2021) 1911–1920, https://doi.org/10.4103/1673-5374.308069.
[74] X.H. Wu, Q.Q. Deng, S.X. Jiang, X.L. Yang, Y.M. Zhong, Distribution of somatostatin receptor 5 in mouse and bullfrog retinas, Peptides 33 (2012) 291–297.
[75] R. Cristiani, C. Petrucci, M. Dal Monte, P. Bagnoli, Somatostatin (SRIF) and SRIF receptors in the mouse retina, Brain Res. 936 (2002) 1–14.
[76] Y. Zhang, N. Wu, Q. Li, X. Hu, L. Wang, J.G. Sun, et al., Neuroprotective effect of the somatostatin receptor 5 agonist L-817,818 on retinal ganglion cells in experimental glaucoma, Exp. Eye Res. 204 (2021) 16.
[77] M. Dal Monte, C. Petrucci, A. Cozzi, J.P. Allen, P. Bagnoli, Somatostatin inhibits potassium-evoked glutamate release by activation of the sst(2) somatostatin receptor in the mouse retina, Naunyn Schmiede Arch. Pharmacol. 367 (2003) 188–192.
[78] R. Amato, M. Dal Monte, M. Lulli, V. Raffa, G. Casini, Nanoparticle-mediated delivery of neuroprotective substances for the treatment of diabetic retinopathy, Curr. Neuropharmacol. 16 (2018) 993–1003.